Annual Sea Level Changes on the North American Northeast Coast: Influence of Local Winds and Barotropic Motions

CHRISTOPHER G. PIECUCH

Atmospheric and Environmental Research, Inc., Lexington, Massachusetts

SÖNKE DANGENDORF

Research Institute for Water and Environment, University of Siegen, Siegen, Germany

RUI M. PONTE

Atmospheric and Environmental Research, Inc., Lexington, Massachusetts

MARTA MARCOS

Mediterranean Institute for Advanced Studies, UIB-CSIC, Esporles, Spain

(Manuscript received 6 January 2016, in final form 10 March 2016)

ABSTRACT

Understanding the relationship between coastal sea level and the variable ocean circulation is crucial for interpreting tide gauge records and projecting sea level rise. In this study, annual sea level records (adjusted for the inverted barometer effect) from tide gauges along the North American northeast coast over 1980–2010 are compared to a set of data-assimilating ocean reanalysis products as well as a global barotropic model solution forced with wind stress and barometric pressure. Correspondence between models and data depends strongly on model and location. At sites north of Cape Hatteras, the barotropic model shows as much (if not more) skill than ocean reanalyses, explaining about 50% of the variance in the adjusted annual tide gauge sea level records. Additional numerical experiments show that annual sea level changes along this coast from the barotropic model are driven by local wind stress over the continental shelf and slope. This result is interpreted in the light of a simple dynamic framework, wherein bottom friction balances surface wind stress in the alongshore direction and geostrophy holds in the across-shore direction. Results highlight the importance of barotropic dynamics on coastal sea level changes on interannual and decadal time scales; they also have implications for diagnosing the uncertainties in current ocean reanalyses, using tide gauge records to infer past changes in ocean circulation, and identifying the physical mechanisms responsible for projected future regional sea level rise.

1. Introduction

Physical oceanographers have long sought to understand the relation between sea level on the northeast coast of North America and ocean dynamics in the North Atlantic. Appealing to simple models of the coastal response (Csanady 1982), earlier studies considered the connection between sea level fluctuations and local atmospheric forcing over the shallow continental shelf. Using two years of data, Sandstrom (1980) reveals a strong link between adjusted sea level (i.e., sea level corrected for the ocean's isostatic adjustment to barometric pressure changes) on the Nova Scotia shoreline and alongshore wind on the Scotian shelf at periods greater than 20 days. This result is interpreted in light of a barotropic model, wherein the momentum balance is between wind stress and bottom drag in the alongshore direction and geostrophic in the across-shore direction. Thompson (1986) investigates sea level changes from long tide gauge records on the western boundary of the North Atlantic north of Cape Hatteras. Thompson (1986) hypothesizes that, while

Corresponding author address: Christopher G. Piecuch, Atmospheric and Environmental Research, Inc., 131 Hartwell Avenue, Lexington, MA 02421.
E-mail: cpiecuch@aer.com

DOI: 10.1175/JCLI-D-16-0048.1

they are partly affected by local air pressure and wind stress, mean sea level anomalies along this coastline are also influenced by changes in a wind-driven, coastally trapped boundary current. Greatbatch et al. (1996) contrast simulations from a homogeneous ocean model forced with air pressure and wind stress to tide gauge data on the North Atlantic western boundary. Greatbatch et al. (1996) discern that the model faithfully reproduces the observed adjusted sea level behavior on synoptic time scales (periods of 3–10 days).

This topic has also enjoyed renewed interest over the last decade, owing to concerns over global climate change and the possibility that the ocean circulation will change and coastal sea level will rise (e.g., Levermann et al. 2005; Landerer et al. 2007; Vellinga and Wood 2008; Yin et al. 2009). Based on geostrophic considerations and freshwater hosing experiments performed with a coarse-resolution model, Levermann et al. (2005) reason that a 1-Sverdrup (Sv; $1\,\mathrm{Sv} \equiv 10^6\,\mathrm{m^3\,s^{-1}}$) decline in the strength of the overturning streamfunction would be accompanied by a 4–5-cm rise in sea level on the North American east coast. Studying an eddy-permitting ocean model, Bingham and Hughes (2009) find a qualitatively similar connection between ocean circulation and coastal sea level, such that a 1-Sv decline in the northward volume transport of the upper (100–1300 m) North Atlantic at 50°N is associated with a 2-cm increase in sea level along the northeast coast of North America. In their study of dynamic sea level projections from coupled climate models, Yin et al. (2009) warn that the United States northeast coast may experience rapid sea level rise over the next century in connection with a potential slowing of the Atlantic meridional overturning circulation.

Motivated by such modeling investigations, more recent studies have taken to the tide gauge record to see whether such mean sea level signatures of ocean circulation changes can be inferred, across a variety of time scales. Sallenger et al. (2012) identify a "hotspot" of accelerated sea level rise on the Atlantic coast of North America—a stretch of coastline from Virginia to Massachusetts along which the rate of sea level rise over the last few decades has been increasing approximately 3–4 times faster than the global average rate. Comparing to previous climate model simulations, Sallenger et al. (2012) suggest that the hotspot is consistent with a downturn in the meridional overturning circulation. Examining solutions from an Earth system model, Yin and Goddard (2013) make the argument that there was an overall northward shift in the Gulf Stream position over the last century, which contributed to coastal tide gauge sea level rise observed along the Mid-Atlantic Bight. Using tide gauge records between New York and Newfoundland, Goddard et al. (2015) determine that there was a striking interannual sea level rise event that recently occurred on the northeast coast of North America, which they partly ascribe to a contemporaneous downturn in the overturning circulation.

These analyses have prompted contemporary investigations to consider in more detail what are the dynamical mechanisms underlying the interannual and decadal sea level changes observed along this shoreline. Andres et al. (2013) determine a significant correlation between a composite of annual coastal sea level anomaly (from tide gauges averaged over the Mid-Atlantic Bight, Gulf of Maine, and Scotian shelf) during the period 1970–2012 and 1) alongshore wind stress locally over the continental shelf and 2) wind stress curl remotely over the Labrador Sea. They interpret their findings qualitatively in light of the barotropic model described by Sandstrom (1980). Woodworth et al. (2014) consider the tide gauge record along the northeastern North American Atlantic coast between Capes Hatteras and Breton Island over 1950–2009, showing a relationship between annual sea level from the data and solutions from the Liverpool/Hadley Centre ocean model driven by winds and thermohaline forcing.[1] In discussing their results, Woodworth et al. (2014) appeal to simple linear models for the response of stratified, frictional flows on the continental shelf to large-scale, low-frequency wind variations (e.g., Csanady 1982; Clarke and Brink 1985), pointing to the importance of baroclinic signals trapped at the coast. Thompson and Mitchum (2014) show significant correlations between interannual sea level from tide gauges on the North Atlantic western boundary over 1952–2001 and contemporaneous time series from the German contribution to Estimating the Circulation and Climate of the Ocean (GECCO) state estimate. Thompson and Mitchum (2014) argue that a coherent mode of interannual sea level variability in this region is ultimately because of Sverdrup flows over the interior of the ocean basin.

While their findings are not necessarily contradictory and may pertain strictly to particular time periods and frequency bands, the authors of these more recent dynamical studies are highlighting very different mechanisms in their interpretations of the tide gauge records. Yet for reconstructing past shifts in the ocean's general circulation (Bingham and Hughes 2009; McCarthy et al. 2015) and anticipating future coastal sea level rise (Landerer et al. 2007; Yin et al. 2009), it is important to

[1] To avoid any confusion (cf. Wunsch 2002), we use "thermohaline forcing" to mean the combination of surface heat and freshwater exchanges.

TABLE 1. Tide gauge records used herein. The completeness is the percentage of years over 1980–2010 for which valid records are available. Tide gauges 1–6 (7–27) are located south (north) of Cape Hatteras (see Fig. 1).

No.	Station name	PSMSL identifier	Lon (°W)	Lat (°N)	Completeness
1	Mayport	316	81.4317	30.3933	65%
2	Fernandina Beach	112	81.465	30.6717	81%
3	Fort Pulaski	395	80.9017	32.0333	97%
4	Charleston Island	234	79.925	32.7817	100%
5	Springmaid Pier	1444	78.9183	33.655	68%
6	Wilmington	396	77.9533	34.2267	97%
7	Duck Pier outside	1636	75.7467	36.1833	77%
8	Lewes (Breakwater Harbor)	224	75.12	38.7817	97%
9	Cape May	1153	74.96	38.9683	100%
10	Atlantic City	180	74.4183	39.355	74%
11	Sandy Hook	366	74.0083	40.4667	90%
12	Bergen Point, Staten Island	1637	74.1417	40.6367	65%
13	New York (The Battery)	12	74.0133	40.7	90%
14	Montauk	519	71.96	41.0483	71%
15	Bridgeport	1068	73.1817	41.1733	94%
16	Nantucket Island	1111	70.0967	41.285	90%
17	New London	429	72.09	41.36	94%
18	Newport	351	71.3267	41.505	100%
19	Woods Hole (WHOI)	367	70.6717	41.5233	87%
20	Providence (State Pier)	430	71.4	41.8067	94%
21	Boston	235	71.0533	42.3533	94%
22	Portland, Maine	183	70.2467	43.6567	97%
23	Yarmouth, Maine	1158	66.1333	43.8333	65%
24	Bar Harbor, Frenchman Bay	525	68.205	44.3917	77%
25	Cutler II	1524	67.2967	44.6417	77%
26	Halifax	96	63.5833	44.6667	74%
27	Eastport	332	66.9817	44.9033	84%

distinguish between the relative contributions of different ocean processes to sea level changes observed in the tide gauge record. With the goal of better understanding coastal sea level behavior, and partly motivated by Andres et al. (2013), who suggest the importance of barotropic dynamics, we study tide gauges, ocean reanalyses, and a barotropic model to address the following questions:

- How well are year-to-year changes in sea level observed by tide gauges along the North American northeast coast reproduced by different ocean circulation models?
- Do barotropic processes contribute importantly to these observed sea level changes?
- What are the relative influences of local wind stress forcing over the shallow continental shelf versus remote wind driving over the deep open ocean?

The rest of this paper is structured as follows: in section 2, we describe methods and materials—namely, the tide gauge data, ocean reanalysis products, and barotropic model solution; in section 3, we assess the skill of the ocean reanalyses and barotropic model in reproducing the tide gauge data; in section 4, model experiments are performed using the barotropic model to determine the roles of local and remote winds; finally, we conclude in section 5 with a discussion of our findings.

2. Methods and materials

a. *Tide gauge records*

To study sea level on the northeast coast of North America, we use annual revised local reference (RLR) records from 27 tide gauges (Table 1). Data were extracted from the Permanent Service for Mean Sea Level (PSMSL) database (Holgate et al. 2013; Permanent Service for Mean Sea Level 2015) on 16 February 2015. For reasons explained below, we study the sea level records over the 31-yr period 1980–2010. The selection criteria satisfied by these records are that the tide gauges are situated along the eastern coast of North America, contain at least 20 years of valid annual sea level values over the study period, and are largely exposed to the open ocean (i.e., not sheltered within large inland estuarine systems such as Chesapeake Bay, Delaware Bay, or the St. Lawrence River). Other recent papers have used very similar subsets of the PSMSL RLR data (Sallenger et al. 2012; Andres et al. 2013; Thompson and Mitchum 2014;

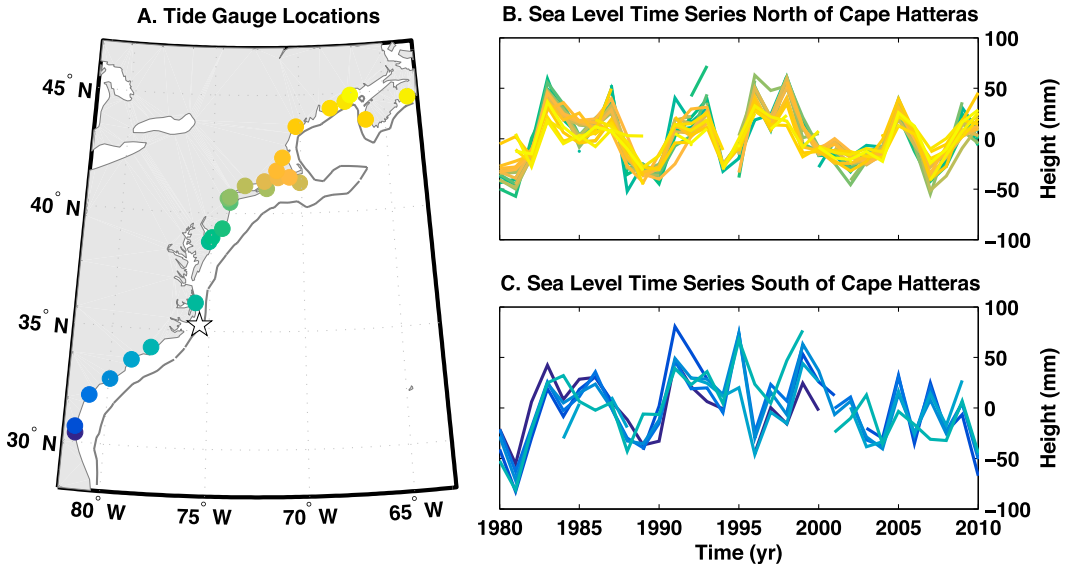

FIG. 1. (a) Color-filled circles show the locations of the 27 PSMSL RLR (Holgate et al. 2013) tide gauges used in this study. The white star denotes Cape Hatteras and the gray contour delineates the 100-m depth. Annual sea level records from those tide gauges (b) north and (c) south of Cape Hatteras, with the colors corresponding to locations in (a). Inverted barometer and linear trend have been removed from the records.

Woodworth et al. 2014; McCarthy et al. 2015). We note that, while our main focus will be on tide gauges along the northeast coast, we have also included some tide gauges along the southeast coast of North America for purposes of comparison (Fig. 1).

Here we focus on changes in dynamic sea level ζ; hence, we adjust the records for isostatic ocean response to barometric pressure (the inverted barometer effect), which can have an important impact on annual sea level changes in this area. For example, Piecuch and Ponte (2015) find that such air-pressure effects explain about 25% of the interannual variance over 1979–2013 and about 50% of the magnitude of an extreme event during 2009/10 in tide gauge records along the northeastern coastline. To estimate the inverted barometer effect, we use annual sea level pressure P_a from the Hadley Centre Sea Level Pressure dataset (Allan and Ansell 2006). We use these P_a data because the PSMSL recommends them as "the most suitable gridded data set ... for sea level studies"[2] [but note that different P_a datasets are very similar in this area over this period and give almost identical results (cf. Fig. 3 in Piecuch and Ponte 2015)]. Data are defined on a regular grid with a horizontal resolution of 5° latitude and longitude over 1850–2012. We assess the inverted barometer effect ζ^{ib} as follows (cf. Ponte 2006):

$$\zeta^{\mathrm{ib}} \doteq -\frac{P_a - \overline{P_a}}{\rho g}, \tag{1}$$

where the overbar denotes the spatial average over the ocean, g is gravity, and ρ is ocean density. Values are mapped to gauge sites using nearest-neighbor interpolation. Given our focus on ocean dynamics, we also remove estimated global mean sea level changes over the period (Church and White 2011).

Similar to recent works by Andres et al. (2013) and Thompson and Mitchum (2014), we restrict our focus to interannual and decadal changes. To isolate these time scales, we remove a linear trend from each of the annual tide gauge records. This serves to filter out changes over longer periods due to global sea level rise and local vertical land motion (Kopp 2013) and possibly also changes in thermohaline forcing and the Atlantic meridional overturning circulation (Yin and Goddard 2013). Consistent with previous studies (e.g., Bingham and Hughes 2009; Thompson and Mitchum 2014; Woodworth et al. 2014), we observe that the coastal ζ anomalies "cluster" into two distinct groups, which are demarcated by Cape Hatteras (Fig. 1). Pairs of tide gauges either north or south of Cape Hatteras are mostly significantly correlated with one another, whereas northern tide gauges do not show statistically significant correlation coefficients with the southern tide gauges (Fig. 2). [Critical values of the correlation coefficient are determined for all pairs of time series based on the autocorrelation properties of the records, following von Storch and Zwiers (1999, section

[2] For example, see http://www.psmsl.org/train_and_info/geo_signals/atm.php.

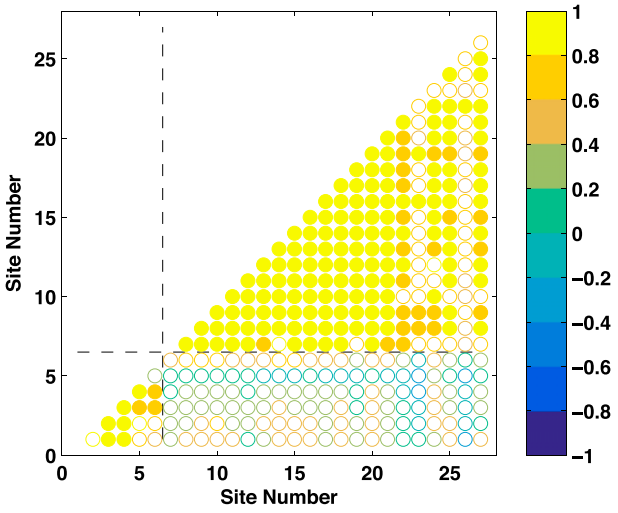

FIG. 2. Correlation coefficient between pairs of annual mean sea level time series. Site numbers correspond to the values given in Table 1. Filled circles are correlation coefficients statistically significant at the 95% confidence level. Critical correlation coefficient values, determined for each pair of time series (von Storch and Zwiers 1999), are usually on the order of 0.6–0.7. The black dashed lines separate sites north and south of Cape Hatteras.

12.4.2).] In what follows, we seek to elucidate the dynamical mechanisms underlying these ζ fluctuations.

b. *Ocean reanalysis products*

To interpret the observed ζ anomalies (Fig. 1), we investigate output from four ocean reanalyses: National Centers for Environmental Prediction (NCEP) Global Ocean Data Assimilation System (GODAS; Behringer and Xue 2004; Xue et al. 2011), Simple Ocean Data Assimilation (SODA) version 2.2.4 (Giese and Ray 2011; Chepurin et al. 2014), the recent synthesis from the second version of the German contribution to Estimating the Circulation and Climate of the Ocean (GECCO2) consortium (Köhl 2015), and the operational Ocean Reanalysis System 4 (ORAS4) taken from the European Centre for Medium-Range Weather Forecasts (ECMWF; Balmaseda et al. 2013). Reanalyses were chosen largely based on their availability and temporal coverage. While each solution assimilates some ocean observations, two of them (GECCO2 and ORAS4) bring in altimetry data away from the coast, and none incorporate tide gauge data. A detailed description of the products is given in the appendix.

We take annual-mean ζ time series from the reanalyses. Since some models may not be faithful right at the coast, especially where the shelf is narrow compared to the model resolution, for each reanalysis and tide gauge, we map the model to the data by selecting the reanalysis ζ time series from the grid cell within a 300-km radius around the gauge site that explains the most variance in the tide gauge record. Analogous methods have been used in recent studies that compare modeled and observational coastal sea level time series (e.g., Calafat et al. 2014; Dangendorf et al. 2014; Chepurin et al. 2014). {While our choice for the radius around the tide gauge is motivated by Chepurin et al. (2014), who use a similar value, we admit that 300 km is somewhat broader than the width of the continental shelf along this coastline [O(100–200) km]. Note, however, that our findings are insensitive to this particular radius choice, and different choices lead us to effectively identical conclusions.} Given the temporal overlaps of the reanalysis products, we study ζ over the common interval 1980–2010. As with the tide gauge records, linear trends have been subtracted from all the reanalysis time series and respective global mean time series have also been removed. (As none of the reanalyses include pressure forcing, no inverted barometer adjustment is needed.)

c. *Barotropic model solution*

To complement our study of tide gauge ζ based on ocean reanalyses, we also use a barotropic[3] model solution generated by the Massachusetts Institute of Technology General Circulation Model (Marshall et al. 1997). We configure the global ocean model to solve the Navier–Stokes equations for a homogeneous ocean driven by P_a and wind stress at the sea surface. The model grid has a nominal horizontal spacing of 1° latitude and longitude using the same topology and bathymetry files as in the Estimating the Circulation and Climate of the Ocean (ECCO) version 4 ocean state estimate (Forget et al. 2015). Since this horizontal resolution is comparable to the width of the shelf in this region, this model cannot be expected to resolve the details of flows near the coast that are strongly constrained by fine topographic features. However, determining the skill of such a model (e.g., in reproducing tide gauge records) is still of interest, as Intergovernmental Panel on Climate Change–class models, used for sea level projections (e.g., Little et al. 2015), employ comparable horizontal grid spacings.

We force the model with surface fields from the ECMWF interim reanalysis (ERA-Interim; Dee et al. 2011), which covers 1979–2015 with a 0.75° latitude–longitude horizontal

[3] The word barotropic has been used variously (and sometimes confusingly) in the physical oceanography and sea level literatures. Generally speaking, a barotropic fluid is one in which the pressure and density surfaces align (e.g., Holton 1992), for example, so that ocean pressure gradients do not generate vorticity (e.g., Pedlosky 1992). Here we use the term in a more restrictive sense to mean a homogeneous ocean with constant density.

grid spacing. A single layer is used in the vertical with variable ocean depths implemented using partial cells (Adcroft et al. 1997). The model uses a linear free surface, no-slip boundary conditions at the bottom and along the sides, a vertical eddy viscosity of $1 \times 10^{-3}\,m^2 s^{-1}$, quadratic bottom drag, and a horizontal eddy viscosity that varies with gridcell size. Observe that, because the model uses only one level in the vertical, the surface wind stress and frictional bottom boundary conditions are cast as body forces that act over the whole fluid column. The barotropic model setup uses a 900-s time step for the momentum equations along with a 3600-s time step for the free surface condition.

The model is started from rest using a 5-yr spinup period. During that time, it is driven with climatological P_a and wind stress, thereafter it is forced with monthly reanalysis fields. While the model uses low-frequency (monthly) forcing, we also performed runs using high-frequency (daily) forcing fields, but they yielded nearly identical annual ζ solutions (not shown) and so are not discussed any further. To be consistent with the tide gauge records and ocean reanalyses, we remove the inverted barometer effect from the barotropic model solution. As with the reanalyses, we match model and data annual ζ fields by taking the nearby model ζ time series that explains the most variance in the tide gauge record. We remove a linear trend during the 1980–2010 period.

3. Comparing models and data

A number of recent papers compare tide gauges to sea level from ocean models in different areas (Dangendorf et al. 2014; Calafat et al. 2014; Chepurin et al. 2014; Thompson and Mitchum 2014; Woodworth et al. 2014). To gain deeper physical insight, we revisit this important topic, examining the tide gauge records and ocean model solutions along the North American northeast coast. To infer how well models reproduce the data, we compute two quantities: 1) the correlation coefficient r and 2) the relative root-mean-square deviation δ between the model and the data, given by

$$\delta \doteq \frac{\sigma(m-d)}{\sigma(d)}, \tag{2}$$

where m and d represent model and data ζ time series, respectively, and σ is standard deviation.

The relationship between the models and the data varies from place to place and from model to model. There are no tide gauge sites at which the ζ data are significantly correlated with the modeled record from GECCO2, ORAS4, or GODAS (Figs. 3b,c,e). Root-mean-square deviations between the data and either GECCO2 or GODAS are relatively large ($\delta \gtrsim 0.9$; Figs. 3g,j). ORAS4 performs only slightly better in this regard, for example, yielding $\delta \sim 0.7$ at Fernandina Beach (Fig. 3h). These results are consistent with Köhl (2015), who shows that GECCO2 has little skill in reproducing altimetric ζ data in this area over 1993–2011. Such poor correlations are surprising, since an earlier GECCO solution shows good correlation over 1952–2001 with tide gauges in this region (Thompson and Mitchum 2014). These findings also accord with Chepurin et al. (2014), who reveal poor correlation between tide gauges and ORAS4 along this coastline over 1950–2008.

The barotropic model and SODA solution show better correspondence to the data along the northeast coast of North America. At most sites north of Cape Hatteras, SODA and the barotropic model both manifest statistically significant correlation coefficients with the tide gauge records (Figs. 3a,d). Additionally, these two solutions give relative root-mean-square deviations with the data that are considerably smaller than δ values based on the three other model products (Figs. 3f,i). However, despite their skill at sites north of Cape Hatteras, neither SODA nor the barotropic model compares well with the tide gauge data along the South Atlantic Bight, evidenced by insignificant correlation coefficients (Figs. 3a,d) and elevated root-mean-square deviations (Figs. 3f,i). Calafat et al. (2014) and Dangendorf et al. (2014) present similar findings, demonstrating that the SODA model captures the annual tide gauge records better north of Cape Hatteras than south of this point.

Because of the alongshore coherence of the tide gauge records (Fig. 2), very similar conclusions regarding model performance follow from comparison of the models and data on larger scales. Figure 4 shows ζ time series from the different model and observational records averaged over the sites either north or south of Cape Hatteras, whereas the correspondence between models and data is summarized by the Taylor diagram (Taylor 2001) shown in Fig. 5. North of Cape Hatteras, SODA and the barotropic model both show significant correlations with the data; however, while the barotropic model underestimates the amplitude of the observed signal, SODA overestimates the observed signal's amplitude. GODAS similarly overestimates the observed magnitude along the northeastern coastline, but this model solution shows poor correlation with the observational time series. South of Cape Hatteras, SODA and GODAS capture the observed signal amplitude, but neither of them is significantly correlated with the observations. Whereas ORAS4 and

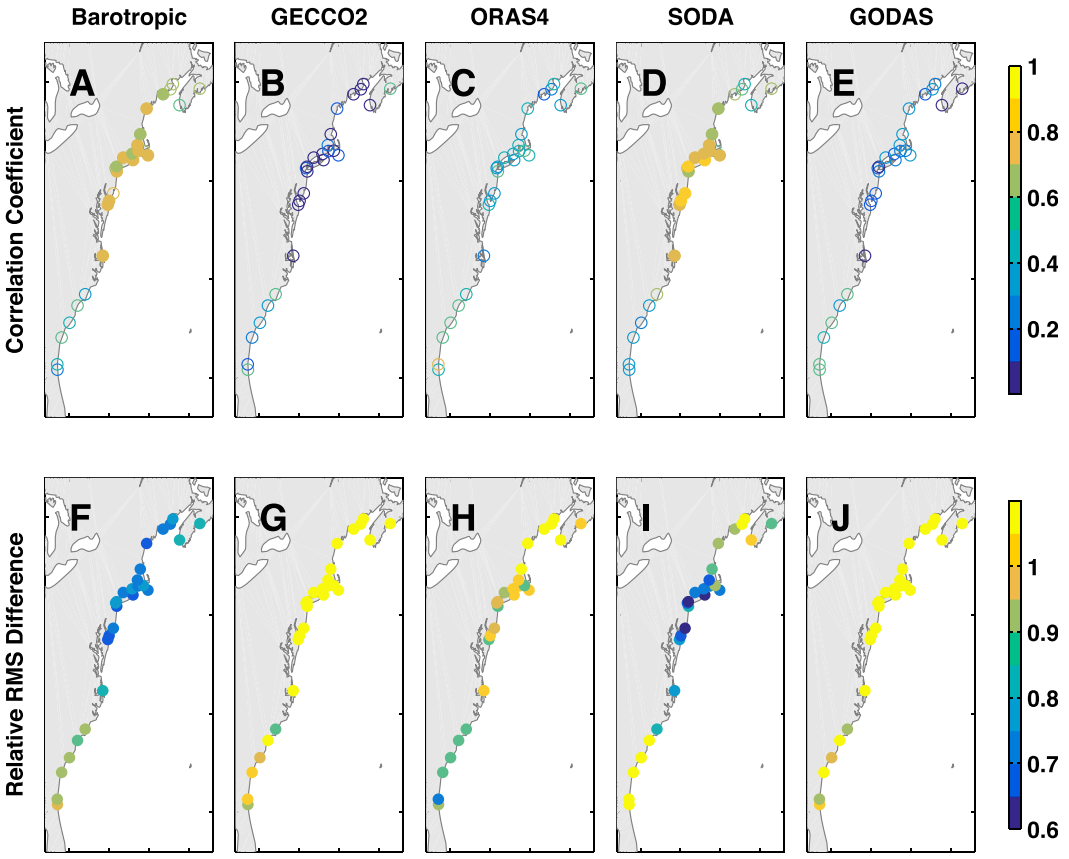

FIG. 3. (a)–(e) Correlation coefficient r and (f)–(j) relative root-mean-square deviation δ between annual tide gauge records and sea level time series from the (a),(f) barotropic model, (b),(g) GECCO2, (c),(h) ORAS4, (d),(i) SODA, and (e),(j) GODAS. Correlation values in (a)–(e) with filled circles are statistically significant at the 95% confidence level (von Storch and Zwiers 1999).

GECCO2 strongly underestimate the amplitude of the composite tide gauge record on the southeast coast, the barotropic model drastically underestimates the magnitude of this tide gauge ζ record (Figs. 4 and 5).

The good correlation between tide gauges and the barotropic model along the northeast coast is consistent with previous studies. Based on a regression analysis, Andres et al. (2013) hypothesize that local winds and barotropic response are important to annual ζ changes along this shoreline. Similarly, Calafat and Chambers (2013) demonstrate that a multiple linear regression involving local wind and sea level pressure can explain a substantial portion of the annual ζ variance at the Boston and New York tide gauges. Moreover, the barotropic model's poor performance south of Cape Hatteras is also in agreement with past works. Based on linear dynamics, Hong et al. (2000) reason that the baroclinic response to open-ocean wind curl by means of Rossby waves is an important contributor to decadal ζ variability along the South Atlantic Bight. Bingham and Hughes (2012), using a high-resolution global ocean circulation model, show that interannual variations in seafloor density along the continental slope and deep ocean have more of an influence on coastal ζ changes south of Cape Hatteras, hence suggesting that there is a stronger decoupling between coastal ζ and deep steric signals to the north of Cape Hatteras. Moreover, numerical experiments considered by Woodworth et al. (2014) hint that thermohaline forcing affects ζ changes south of Cape Hatteras.

In summary, our results show that ocean models differ in their ability to reproduce annual ζ changes observed on the North American east coast. They also suggest that barotropic processes contribute appreciably to interannual and decadal ζ variance on the coast north of Cape Hatteras. To elucidate the relevant barotropic dynamics, in the section that follows we report on results from additional numerical forcing simulations that were performed based on the barotropic model setup.

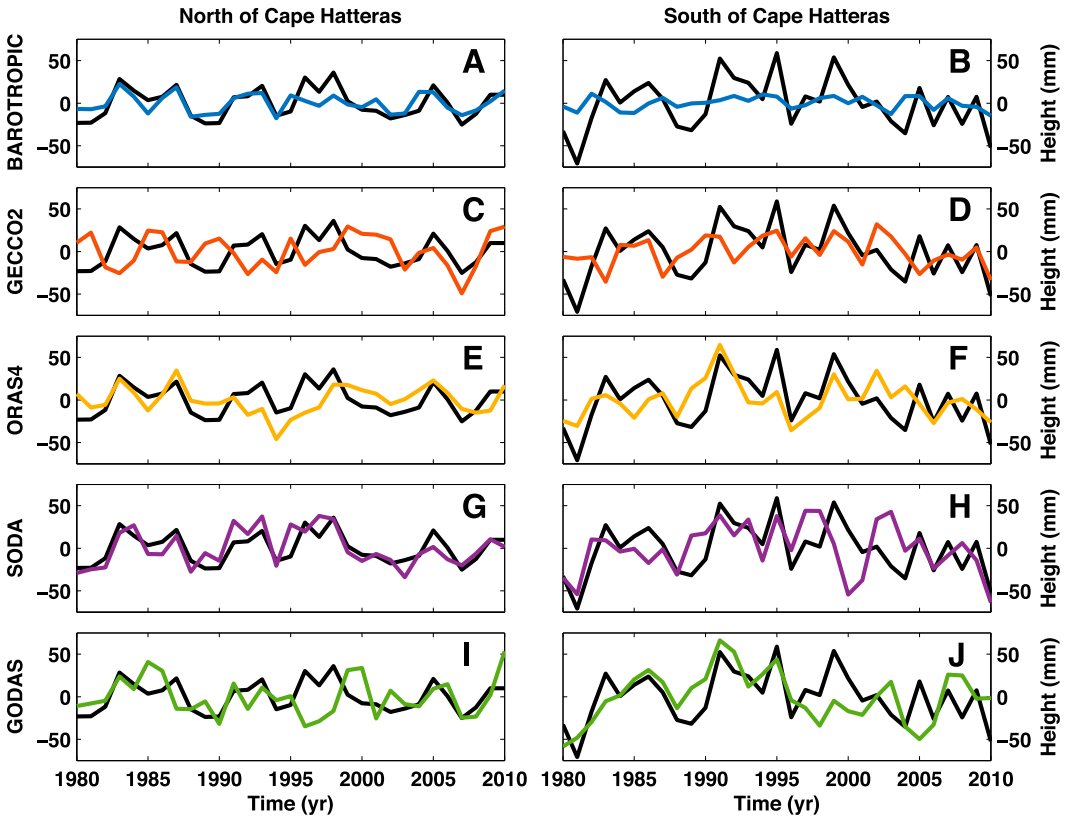

FIG. 4. Observed and modeled sea level averaged over tide gauges (left) north or (right) south of Cape Hatteras. (See Fig. 1a for locations.) The black curves are the tide gauge time series while the colored curves indicate the various model solutions: (a),(b) the barotropic model (blue), (c),(d) GECCO2 (orange), (e),(f) ORAS4 (yellow), (g),(h) SODA (purple), and (i),(j) GODAS (green).

4. Forcing experiments and dynamical interpretation

Our simple barotropic model solution performs as well as, if not better than, other more complete (and data assimilating) ocean general circulation model frameworks with regard to reproducing annual tide gauge observations along the northeast coast of North America. This demonstrates that more complex models do not necessarily produce more realistic solutions. In the most general terms, the ζ signals from the barotropic model can reflect dynamic ocean response to barometric pressure and wind stress locally as well as remotely. To reveal the roles of local and remote wind and pressure, we conduct the following experiments based on the barotropic model configuration:

- In the PRES experiment, we again run forward the barotropic model as described previously, but we turn off the wind stress surface forcing. Hence, once corrected for the inverted barometer effect, this solution represents the dynamic ocean response to barometric pressure.
- For the SHAL run, we set to zero barometric pressure and wind stress over the deep ocean, leaving the wind stress over the shelf and slope ($<$1000 m) as the only driver of ζ variability.
- Similar to SHAL, for the DEEP run we remove pressure and wind forcing over the shallow ocean from this simulation, allowing only wind stress over the deep ocean ($>$1000 m) to force the model.

In all other respects (e.g., initial conditions), these perturbation runs are identical to the original barotropic ocean model simulation, which hereafter we refer to as the BASE experiment for clarity.

The outcomes of the experiments are summarized in Fig. 6, which compares ζ time series from the BASE, PRES, DEEP, and SHAL simulations averaged over the tide gauge sites north of Cape Hatteras. [Because of the strong spatial coherence of the signals (Fig. 2), analogous conclusions follow from comparing the different barotropic model experiments at the various individual tide gauges (not shown).] The PRES experiment evidences no appreciable dynamic behavior in this region and explains none of the ζ variance from the BASE

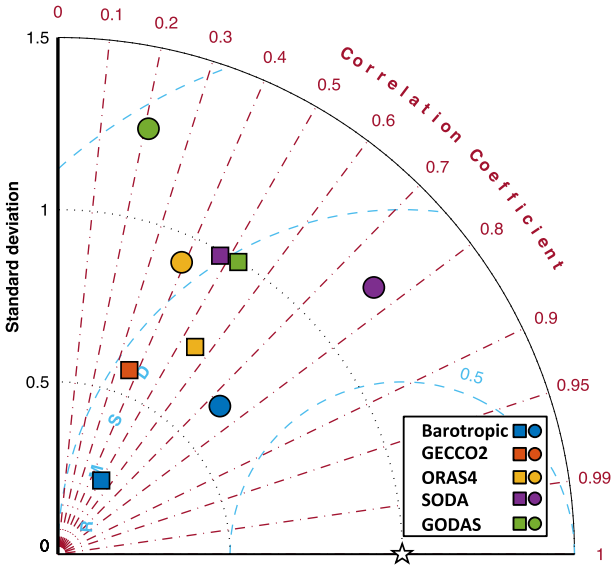

FIG. 5. Taylor diagram summarizing the correspondence between tide gauge records averaged north (circles) and south (squares) of Cape Hatteras and the corresponding sea level time series from the barotropic model (blue), GECCO2 (orange), ORAS4 (yellow), SODA (purple), and GODAS (green). Along the radial coordinate of the diagram is shown the standard deviation of the simulated ζ record divided by the standard deviation of the corresponding observational time series, along the azimuthal coordinate is shown the correlation coefficient r between the modeled and observed time series, and emanating from the reference point [i.e., the coordinate pair (1, 1) denoted by the star in the diagram] is the relative root-mean-square deviation δ between the model and gauge records. The only significant correlation values are those from SODA and the barotropic model north of Cape Hatteras. (Note that the orange circle, corresponding to the performance of the GECCO2 product north of Cape Hatteras, is not missing from the figure but rather falls outside the axis limits, because of the negative correlation coefficient.)

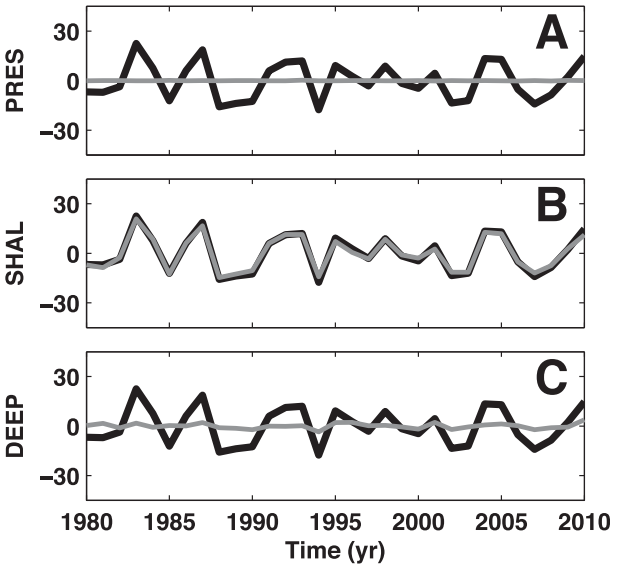

FIG. 6. Annual sea level (mm) averaged over 20 tide gauges north of Cape Hatteras from the different barotropic model runs: (a) PRES, (b) SHAL, and (c) DEEP. Black curves in each panel are identical and represent the sea level time series from the original simulation (BASE). Gray curves in the different panels are the sea level changes averaged over the sites from the different forcing experiments.

simulation (Fig. 6a). This result is not surprising, as the barotropic oceanic adjustment to pressure loading at these space and time scales is expected to be mainly isostatic and mostly explained by the inverted barometer response (e.g., Ponte 1993).

In sharp contrast, the ζ time series from the SHAL and BASE experiments are nearly identical—the correlation coefficient between them is 0.99 (Fig. 6b). This suggests that annual barotropic ζ fluctuations along the coast are driven by wind stress over the shelf and slope. The ζ fluctuations from the SHAL experiment are almost perfectly anticorrelated (correlation coefficient of -0.99) with the local alongshore wind stress over the Mid-Atlantic Bight, Gulf of Maine, and Scotian shelf (Fig. 7a). Andres et al. (2013) also find strong anticorrelation between alongshore wind stress and coastal sea level, but the relation shown in Fig. 7a is much stronger than the one they see (cf. Fig. 4b in Andres et al. 2013), likely because, as we use the barotropic component from the model rather than tide gauge data, we have effectively removed the influence of wind stress over the deep ocean and barometric pressure.

Sandstrom (1980) provides a physical framework for interpreting this antiphase relationship between sea level and alongshore wind stress. Consider a shelf of width W and depth H along the coast. Suppose that the momentum balance in the alongshore direction (here $\hat{y}$) is between wind stress and bottom friction, and say that geostrophy holds in the across-shore direction $\hat{x}$:

$$-fv = -g\frac{\partial \zeta}{\partial x} \quad \text{and} \tag{3}$$

$$\frac{\tau_y}{\rho H} = 2\frac{A_v}{H}v, \tag{4}$$

where f is the Coriolis parameter, g is the gravitational acceleration, v and τ_y are the alongshore (i.e., meridional) velocity and wind stress, respectively, and A_v is vertical eddy viscosity.[4] If we assume that alongshore wind stress is constant, integrate across the shelf, and make

[4] This form of vertical dissipation (i.e., with the prefactor of two and inverse dependence on depth) is chosen to be consistent with the formulation of the no-slip bottom condition in the model (e.g., see Adcroft et al. 2016, section 2.14.6), where we ignore quadratic bottom drag for simplicity.

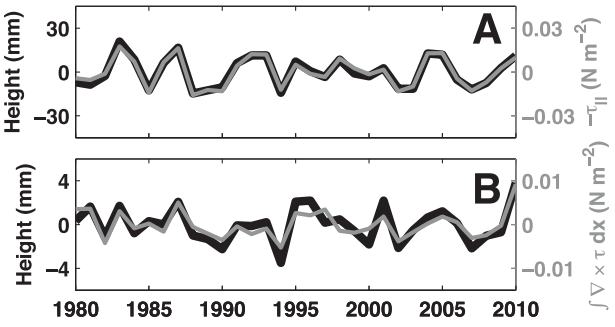

FIG. 7. (a) Sea level from SHAL averaged over the 20 tide gauge sites north of Cape Hatteras (black) vs the negative of the average alongshore wind stress (denoted as $-\tau_{\|}$) over the northeastern continental shelf (gray). We define the alongshore wind stress as the inner product between wind stress vector $\boldsymbol{\tau} = (\tau_x, \tau_y)$ and an alongshore unit vector $\mathbf{n} = (\cos\vartheta, \sin\vartheta)$, where we have chosen $\vartheta = 30°$. We define the extent of the northeastern continental shelf as the region within 53°–100°W and 35°–45°N where the ocean depth is less than 1000 m. (b) Sea level from DEEP averaged over the 20 tide gauge sites north of Cape Hatteras (black) vs wind stress curl integrated zonally across the deep ocean (>1000 m) and averaged over 35°–45°N (gray). All the time series are detrended.

substitutions with the equations, we obtain the following relation between sea level and alongshore wind stress:

$$\Delta\zeta^{+} = \frac{fW}{2A_{\nu}\rho g}\tau_{y}, \tag{5}$$

where $\Delta\zeta^{+}$ is the difference between coastal and offshore (i.e., at the edge of the shelf) sea level. Choosing values representative for the shelf along the North American northeast coast in the model ($f \approx 10^{-4}\,\mathrm{s}^{-1}$, $W \approx 200\,\mathrm{km}$, $A_{\nu} \approx 10^{-3}\,\mathrm{m}^2\,\mathrm{s}^{-1}$, $\rho \approx 10^{3}\,\mathrm{kg\,m}^{-3}$, and $g \approx 10\,\mathrm{m\,s}^{-2}$) and supposing that sea level vanishes at the oceanward edge of the shelf, we find that Eq. (5) gives us a constant of proportionality between coastal sea level and alongshore wind stress of roughly $-1\,\mathrm{m}^3\,\mathrm{N}^{-1}$. This is very close to what we actually find in the SHAL experiment (Fig. 7a), and moreover it is consistent with the range given by Andres et al. (2013), which suggests that the barotropic mechanism described by Sandstrom (1980) and appealed to by Andres et al. (2013) is in fact an important contributor to interannual and decadal ζ change on the North American northeast coast.

Consistent with these findings, barotropic response to wind driving over the deep ocean has only a small influence, with ζ along the northeast coast from the DEEP experiment amounting to just about 15% of the coastal ζ variance from the BASE simulation (Fig. 6c). (The ζ signals from the SHAL and DEEP experiments covary, so their variances are not additive.) The ζ changes on the coast from the DEEP simulation are correlated (correlation coefficient of approximately −0.9) with wind stress curl forcing integrated zonally over the deep basin (Fig. 7b). Such a relationship between the coastal sea level and wind stress curl variations is anticipated in case of a barotropic Sverdrup balance; specifically,

$$\Delta\zeta^{-} = -\frac{f}{gD\beta\rho}\int \nabla\times\tau\, dx, \tag{6}$$

where $\Delta\zeta^{-}$ is the zonal difference in sea level across the ocean basin, β is the meridional derivative of f, D represents the depth of the deep ocean, and $\nabla\times\tau$ is the vertical component of the wind stress curl. (Here we have also assumed a β-plane ocean with a flat bottom.) Now supposing that ζ vanishes at the eastern boundary of the basin and using order-of-magnitude parameter values ($f \approx 10^{-4}\,\mathrm{s}^{-1}$, $D \approx 4000\,\mathrm{m}$, $\beta \approx 10^{-11}\,\mathrm{m}^{-1}\,\mathrm{s}^{-1}$, $\rho \approx 10^{3}\,\mathrm{kg\,m}^{-3}$, and $g \approx 10\,\mathrm{m\,s}^{-2}$), we obtain a constant of proportionality between northeast coast sea level and the zonally integrated wind stress curl of about $0.25\,\mathrm{m}^3\,\mathrm{N}^{-1}$, which is on the order of what we see in the DEEP simulation (Fig. 7b), suggesting that barotropic Sverdrup balance is a plausible mechanism explaining this relationship.

5. Discussion

Previous investigations have studied the relation between coastal sea level and ocean circulation changes in observations of the past as well as projections of the future (e.g., Landerer et al. 2007; Bingham and Hughes 2009; Yin et al. 2009; Andres et al. 2013; McCarthy et al. 2015). Motivated by such works, we considered annual tide gauge sea level records along the North American east coast over the 1980–2010 period (Figs. 1 and 2); these records were interpreted using different ocean circulation model solutions. We found that the correspondence between the data and models depends strongly on region and model—none of the models faithfully reproduce the coastal sea level changes observed south of Cape Hatteras, and only some models skillfully capture coastal sea level behavior measured north of Cape Hatteras (Figs. 3–5). Interestingly, we saw that a simple barotropic ocean model performed as well as (if not better than) more complex ocean reanalyses, which incorporate effects of buoyancy forcing and ocean stratification; this was apparent at tide gauge locations north of Cape Hatteras, where the barotropic model generally explains about 50% of the variance in the observational sea level records (Figs. 3 and 5). Using this same barotropic ocean model framework, we also performed additional numerical simulations, variously driving the model with wind stress or barometric pressure over different ocean regions (Figs. 6 and 7). Based on those experiments, we reasoned that anomalous alongshore wind stress is the dominant driver of

barotropic sea level variations along the North American northeast coast on these time scales (Figs. 6b and 7a); less relevant in this instance is wind curl forcing over the deep open ocean (Fig. 6c).

These findings improve our understanding of coastal sea level behavior and generally accord with previous works. Based on correlation and regression analyses, Andres et al. (2013) argue that a considerable portion of annual sea level variance in this region is controlled by local alongshore wind stress, consistent with what we found here (Figs. 4a and 6b). The numerical model experiments performed by Woodworth et al. (2014) hint that wind forcing contributes more to the coastal sea level variance north of Cape Hatteras than it does to the south (see Fig. 6 in Woodworth et al. 2014). This is in rough agreement with our results, suggesting that coastal sea level dynamics are distinct north and south of Cape Hatteras, with barotropic processes being more influential at locations north of this site than they are to the south (e.g., Fig. 4). However, we note that our results on this point contrast with the conclusions drawn by Yin and Goddard (2013) that baroclinic processes control dynamic sea level changes to the north of Cape Hatteras and barotropic effects dominate south of this point.

More generally, our conclusions corroborate previous global ocean modeling efforts suggesting that sea level and bottom pressure can be strongly coupled on shallow-shelf sea regions even on interannual and longer time scales (Vinogradova et al. 2007; Bingham and Hughes 2008). However, we emphasize that the local barotropic mechanisms highlighted in this study account for roughly one-half of the dynamic sea level variance along the northeast coast of North America (Figs. 3 and 5), leaving a substantial fraction of the adjusted tide gauge variance to be explained. Indeed, similar to the adjusted tide gauge records (Fig. 2), the residual time series (i.e., adjusted tide gauges minus barotropic model solution) evidence broad spatial coherence along the coast (not shown); these residual time series show significant correlation with the adjusted tide gauge records but are not significantly correlated with the barotropic model solutions (not shown). These results possibly implicate mechanisms emphasized in other studies, for example, zonal flows across the 65°W meridian (Thompson and Mitchum 2014) or baroclinic signals trapped at the coast (Woodworth et al. 2014).

We also performed various analyses (wavelet coherence, spectral analysis, etc.) in the frequency domain (not shown). The tide gauge and barotropic model sea level time series north of Cape Hatteras show stronger coherence at higher (interannual) frequencies and weaker coherence at lower (decadal) frequencies. Indeed, although removing the barotropic model solution reduces the spectral power of the tide gauge data at all frequencies, the residual difference between them is slightly red. These findings are in accord with the basic theory of the oceanic response (e.g., Gill and Niiler 1973; Frankignoul et al. 1997), which says that ocean stratification effects become more important with decreasing frequency. Additionally, the relationship between tide gauge and barotropic model sea level north of Cape Hatteras seems not to be stationary. For example, the correlation coefficient between these two time series is 0.91 for the decade 1983–93 but 0.43 for the decade 1994–2004. Somewhat similarly, Andres et al. (2013) find that the correspondence between northeast coast sea level and the North Atlantic Oscillation was stronger during 1987–2012 than during 1970–86. This emphasizes that results here apply only to the time periods and frequency bands considered.

It is disconcerting that some ocean reanalysis products perform so poorly on this coastline (Figs. 3 and 5). For them to yield meaningful projections of future coastal sea level change, models must be able to represent processes at the boundaries and capture the coupling between sea level over the deep ocean and the shallow shelf (cf. Higginson et al. 2015; Hughes et al. 2015; Saba et al. 2016). To that end, understanding the reasons for the dispersion in model performance (Fig. 5) is imperative. Based on our findings (Figs. 6 and 7), good estimates of local alongshore wind stress seem to be crucial for accurate simulations of sea level changes on the North American northeast coast. This suggests that the observed dispersion in model skill (Figs. 3–5) might be partly due to the different wind stress forcing fields used by the various models over this region. To assess this suggestion, we took alongshore wind stress time series over the North American northeast shelf from different atmospheric reanalysis products—including all those used as surface forcing in the ocean models considered here (see the appendix)—and compared them to the annual tide gauge sea level records averaged over this coastline (Fig. 8). We found that all alongshore wind stress products are significantly anticorrelated with the tide gauge records; after multiplying by the scale factor of $-1\,\mathrm{m^3\,N^{-1}}$ determined in the last section, the reanalysis wind stress time series explain 44%–55% of the annual variance in the tide gauge sea level record, depending on the choice of atmospheric reanalysis. This suggests that uncertainties in alongshore wind stress and local barotropic response are probably not responsible for the discrepancies in the skills of the different ocean models in this region (Fig. 5); rather, these discrepancies must be due to inaccurate representation of some other forcing or process (e.g., thermohaline forcing, ocean stratification, baroclinic response, etc.).

Based on global analyses, Hernandez et al. (2014) and Balmaseda et al. (2015) find that models that assimilate

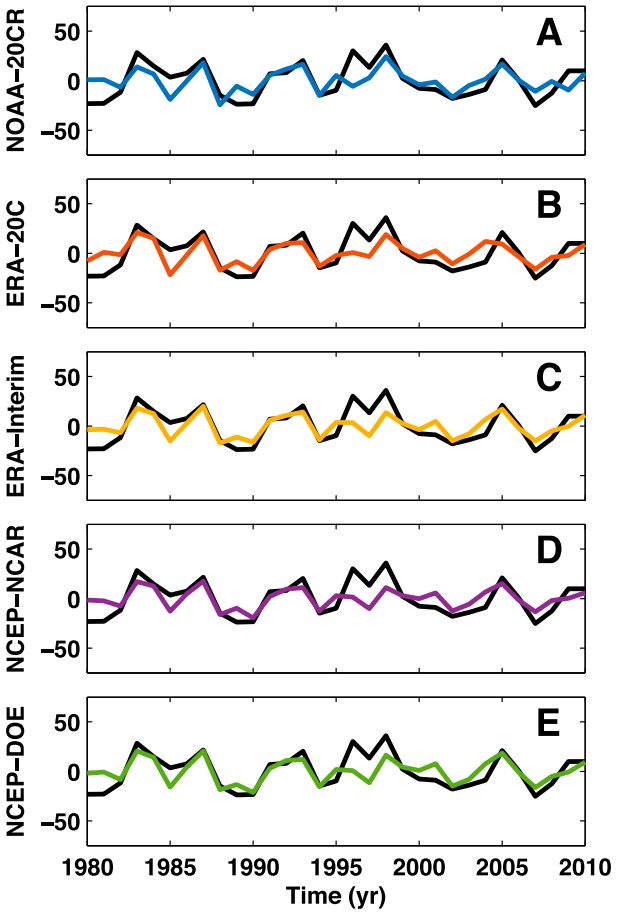

FIG. 8. Sea level and alongshore wind on the northeast coast. Colored curves are the sea level (mm) predicted by averaging detrended annual alongshore wind stress anomalies over the shelf from various atmospheric reanalyses and scaling by $-1\,\mathrm{m^3\,N^{-1}}$ (see the text for more details): (a) NOAA 20CR (blue; Compo et al. 2011), (b) ECMWF twentieth-century reanalysis (ERA-20C, orange; Poli et al. 2013), (c) ERA-Interim (yellow; Dee et al. 2011), (d) NCEP Reanalysis-1 (purple; Kalnay et al. 1996), and (e) NCEP Reanalysis-2 (green; Kanamitsu et al. 2002). The black curve in each panel is observed sea level record (mm) averaged over the 20 tide gauges north of Cape Hatteras (cf. Fig. 1a). We define alongshore wind stress and shelf extent as in Fig. 6.

altimetric data and have finer resolution generally reproduce tide gauge records better than solutions that either are more coarse or do not utilize altimetry. Thus, it might appear strange that the two models studied here that do incorporate altimetry (i.e., ORAS4 and GECCO2) perform poorly compared to other models that do not bring in this dataset (e.g., SODA).[5] However, it must be kept in mind (see the appendix) that neither ORAS4 nor GECCO2 uses altimetric data near land. Notwithstanding concerns over potentially degraded quality of satellite altimetry data near the coast, the correspondence between standard altimetric products and tide gauge records can be good in some coastal regions (e.g., Vinogradov and Ponte 2011), and so it could be that the assimilation methods are discarding valuable data at the coast. Indeed, as specially tailored coastal altimetry products (e.g., Passaro et al. 2015) come online and become more readily available, it will be important to bring them into ocean reanalyses for better representation of the coastal ocean.

Another consideration is that representation of bathymetry could affect the model performance. This point might be especially relevant south of Cape Hatteras, where the coupling of the deep sea and coastal ocean appears to be stronger and where accurate representation of bathymetric gradients could be very important for communicating the influence of deep steric signals on coastal sea level (cf. Bingham and Hughes 2012). However, this issue might not be such a critical factor north of Cape Hatteras, seeing as GECCO2 (which performs poorly along this region) and our barotropic model (which does well in this area) use the same coastline and bathymetry input files. In any case, definitive determination of underlying causes for model discrepancies is beyond our scope; future works should focus in more detail on understanding such poor model performances.

Our results have other implications for interpreting past sea level changes and projecting future sea level rise. We have interpreted the coastal sea level behavior from the barotropic model in light of a framework similar to Sandstrom (1980)—bottom friction balances the wind stress in the alongshore direction, and geostrophy holds in the across-shore direction. This reasoning implies that these tide gauge records can be partly interpreted in terms of alongshore flow. For example, coastal sea level anomalies of 1–2 cm over a 200-km-wide shelf would correspond to variations of 0.5–$1.0\,\mathrm{cm\,s^{-1}}$ in barotropic alongshore geostrophic currents, which amounts to 4%–14% of mean flows observed along the southwest Nova Scotian shelf (e.g., Hannah et al. 2001; Li et al. 2014).

Previous works consider projected overturning circulation changes and their bearing on coastal sea level rise (e.g., Landerer et al. 2007; Yin et al. 2009). Our results hint that future alongshore wind behavior should also be factored into such sea level rise scenarios. With this in mind, we considered projections of alongshore wind stress averaged over the North American

[5] The performances of these reanalyses that assimilate altimetry are not made any better if only the period 1993–2010 is considered (cf. Fig. 4).

northeastern continental shelf from 1% yr^{-1} CO_2 increase experiments (1pctCO2) from 29 coupled climate models as part of phase 5 of the Coupled Model Intercomparison Project (CMIP5; Taylor et al. 2012). We found that, while projected alongshore wind stress trends are mostly not statistically significant, some models do give significant positive trends, amounting to an increase of 0.01–0.02 N m^{-2} over 140 years (not shown). Based on reasoning in the preceding section [Eq. (5)], this corresponds to a sea level drop of 1–2 cm along this stretch of coastline, which is small compared to the regional sea level rise anticipated during this century (e.g., Kopp et al. 2014; Slangen et al. 2014). We also found that, for a great majority (93%) of models considered, there is no significant change in the interannual alongshore wind stress variance over the duration of the simulation (not shown).

Goddard et al. (2015) examine tide gauge records on the northeast coast of North America and reveal an extraordinary rise in annual sea level between 2008 and 2010. Considering transport data, climate models, and an ocean data assimilation product, those authors conclude that this extreme sea level fluctuation was related to a contemporaneous downturn in the overturning circulation and wind stress anomalies associated with strong values of the North Atlantic Oscillation. Taken together with the findings of Piecuch and Ponte (2015), our barotropic model runs (Figs. 4a, 6b, and 7a) suggest that this sea level rise event can be understood almost entirely in terms of the dynamic and isostatic ocean responses to local meteorological conditions over the shelf. This emphasizes that, while sea level and ocean circulation are correlated (e.g., Bingham and Hughes 2009), the Atlantic meridional overturning circulation is not directly coupled to observed sea level changes along the North American northeast coast over these time scales. However, as suggested by one reviewer, this does not preclude a more indirect link to the overturning circulation. For instance, Bryden et al. (2014) argue that the sharp reduction in the overturning circulation (and associated meridional heat transport) during 2009/10 leads to an anomalous atmospheric state over the North Atlantic sector, whose influence was subsequently felt at the coast (cf. Goddard et al. 2015). In any case, the extent to which overturning circulation and coastal sea level changes share common forcing, result from distinct (but still simultaneous) mechanisms, or are intimately coupled through complex ocean–atmosphere interactions should be explored in more detail in future investigations.

We have focused on sea level along the northeast coast of North America on interannual and decadal time scales. However, other studies point to interesting sea level behavior on this shoreline on multidecadal periods. For example, Chambers et al. (2012) reveal a prominent multidecadal fluctuation in the New York and Baltimore tide gauge records; these authors generally suggest that redistribution by oceanic Rossby or Kelvin waves may contribute to such regional sea level signals. Analogously, based on a lagged correlation analysis considering European tide gauges, Miller and Douglas (2007) suggest that westward wave propagation could result in multidecadal sea level oscillations at tide gauges between Halifax and Baltimore. However, it remains to be determined how important variations in more local meteorological conditions are to multidecadal sea level changes along the coast. These important questions are beyond our current scope and left for future study.

Acknowledgments. Author support came partly from NASA Grant NNX14AJ51G. We thank Gaël Forget and Patrick Heimbach for providing the model setup with grid topology and bathymetry files. We acknowledge Ayan Chaudhuri and Chris Little for making available the CMIP5 solutions. The SODA sea level fields were provided by Ligang Chen, Gennady Chepurin, and James Carton. Armin Köhl and Yan Xue also made helpful clarifications regarding some of the ocean reanalyses. We also appreciate the constructive criticisms of Kathy Donohue and three anonymous reviewers.

APPENDIX

Description of Ocean Reanalysis Products

The SODA solution spans 1871–2010 and is defined on a grid with a 0.4° × 0.25° horizontal spacing and 40 vertical levels. (Fields are provided interpolated onto a regular 0.5° latitude–longitude horizontal grid.) Observations of ocean temperature and salinity from the *World Ocean Database 2009* (Boyer et al. 2009) and sea surface temperature from the International Comprehensive Ocean–Atmosphere Data Set release 2.5 (Woodruff et al. 2011) are assimilated using the sequential scheme described by Carton and Giese (2008). Forcing fields are based on NOAA 20CR (Compo et al. 2011), and the ocean model is based on the Parallel Ocean Program (POP) version 2.0.1 (Smith et al. 1992).

The GODAS product covers 1980–2015. It is defined on a quasi-global (75°S–65°N) ocean grid with a nominal lateral resolution of 1° latitude and longitude (but reducing to ⅓° in the tropics) and 40 levels in the vertical.

Using a three-dimensional variational data assimilation (3DVAR) method, this solution incorporates Reynolds sea surface temperature and in situ temperature from expendable bathythermographs, profiling floats, and moorings from the Tropical Atmosphere Ocean (TAO) project, but not altimetry. The basic forcing fields are surface fluxes of momentum, heat, and freshwater from the NCEP Reanalysis-2 (Kanamitsu et al. 2002), and the baseline ocean general circulation model is the Geophysical Fluid Dynamics Laboratory (GFDL) Modular Ocean Model (MOM) version 3.

The ORAS4 solution spans 1958–2014 and is defined on a tripolar spatial grid, which has a nominal horizontal spacing of 1° latitude and longitude, telescoping to 0.3° near the equator, with 42 vertical levels. It is generated using the Nucleus for European Modelling of the Ocean (NEMO) model (Madec 2008) and assimilates Reynolds surface temperature, satellite ζ, and temperature and salinity data from the Enhanced Ocean Data Assimilation and Climate Prediction (ENACT), version 3 (EN3), bias-corrected database (Ingleby and Huddleston 2007) using the NEMO variational data assimilation (NEMOVAR) method described by Mogensen et al. (2012) and with a 10-day assimilation window; a noteworthy aspect of this methodology is that the influence of observational data (including altimetry) on the solution is deemphasized in more coastal ocean regions (Mogensen et al. 2012). Surface temperature and sea ice information are used along with a Newtonian relaxation scheme to constrain the upper levels. The atmospheric forcing until 1989 is from the 40-yr ECMWF Re-Analysis (ERA-40; Uppala et al. 2005), over 1989–2010 from the ECMWF interim reanalysis (ERA-Interim; Dee et al. 2011), and from 2010 onward from the ECMWF operational archive (Balmaseda et al. 2013).

The GECCO2 product is a global ocean state estimate over the period 1948–2011. It is defined on a spatial grid with nominal 1° latitude–longitude spacing but reducing to ⅓° close to the equator and effectively 40 km in the Arctic. (Interpolated solutions are provided on a regular 1° grid.) This solution is generated using the Massachusetts Institute of Technology General Circulation Model (MITgcm; Marshall et al. 1997). It employs the adjoint (or 4DVAR) method to incorporate various satellite and in situ measurements, including AVISO along-track ζ, mean dynamic topography, sea surface temperature from the AMSR-E satellite mission and the Hadley Centre Sea Ice and Sea Surface Temperature dataset (Rayner et al. 2003), and subsurface temperature and salinity from the EN3 database (Ingleby and Huddleston 2007). Note that altimetric ζ fields are assimilated into the estimate only over regions deeper than 130 m. Bulk formulas are used for the adjusted surface forcing fields, which are based on the NCEP Reanalysis-1 (Kalnay et al. 1996; Kistler et al. 2001).

REFERENCES

Adcroft, A., C. Hill, and J. Marshall, 1997: Representation of topography by shaved cells in a height coordinate ocean model. *Mon. Wea. Rev.*, **125**, 2293–2315, doi:10.1175/1520-0493(1997)125<2293:ROTBSC>2.0.CO;2.

——, and Coauthors, 2016: MITgcm user manual. MIT Dept. of Earth, Atmospheric and Planetary Sciences Rep., 481 pp. [Available online at http://mitgcm.org/public/r2_manual/latest/online_documents/manual.pdf.]

Allan, R., and T. Ansell, 2006: A new globally complete monthly historical gridded mean sea level pressure dataset (HadSLP2): 1850–2004. *J. Climate*, **19**, 5816–5842, doi:10.1175/JCLI3937.1.

Andres, M., G. G. Gawarkiewicz, and J. M. Toole, 2013: Interannual sea level variability in the western North Atlantic: Regional forcing and remote response. *Geophys. Res. Lett.*, **40**, 5915–5919, doi:10.1002/2013GL058013.

Balmaseda, M. A., K. Mogensen, and A. T. Weaver, 2013: Evaluation of the ECMWF ocean reanalysis system ORAS4. *Quart. J. Roy. Meteor. Soc.*, **139**, 1132–1161, doi:10.1002/qj.2063.

——, and Coauthors, 2015: The ocean reanalysis intercomparison project (ORA-IP). *J. Oper. Oceanogr.*, **8** (Suppl.), S80–S97, doi:10.1080/1755876X.2015.1022329.

Behringer, D. W., and Y. Xue, 2004: Evaluation of the global ocean data assimilation system at NCEP: The Pacific Ocean. *Eighth Symp. on Integrated Observing and Assimilation Systems for Atmosphere, Oceans, and Land Surface*, Seattle, WA, Amer. Meteor. Soc., 2.3. [Available online at https://ams.confex.com/ams/84Annual/techprogram/paper_70720.htm.]

Bingham, R. J., and C. W. Hughes, 2008: The relationship between sea-level and bottom pressure variability in an eddy permitting ocean model. *Geophys. Res. Lett.*, **35**, L03602, doi:10.1029/2007GL032662.

——, and ——, 2009: Signature of the Atlantic meridional overturning circulation in sea level along the east coast of North America. *Geophys. Res. Lett.*, **36**, L02603, doi:10.1029/2008GL036215.

——, and ——, 2012: Local diagnostics to estimate density-induced sea level variations over topography and along coastlines. *J. Geophys. Res.*, **117**, C01013, doi:10.1029/2011JC007276.

Boyer, T. P., and Coauthors, 2009: *World Ocean Database 2009*. NOAA Atlas NESDIS 66, 216 pp.

Bryden, H. L., B. A. King, G. D. McCarthy, and E. L. McDonagh, 2014: Impact of a 30% reduction in Atlantic meridional overturning during 2009–2010. *Ocean Sci.*, **10**, 683–691, doi:10.5194/os-10-683-2014.

Calafat, F. M., and D. P. Chambers, 2013: Quantifying recent acceleration in sea level unrelated to internal climate variability. *Geophys. Res. Lett.*, **40**, 3661–3666, doi:10.1002/grl.50731.

——, ——, and M. N. Tsimplis, 2014: On the ability of global sea level reconstructions to determine trends and variability. *J. Geophys. Res. Oceans*, **119**, 1572–1592, doi:10.1002/2013JC009298.

Carton, J. A., and B. S. Giese, 2008: A reanalysis of ocean climate using Simple Ocean Data Assimilation (SODA). *Mon. Wea. Rev.*, **136**, 2999–3017, doi:10.1175/2007MWR1978.1.

Chambers, D. P., M. A. Merrifield, and R. S. Nerem, 2012: Is there a 60-year oscillation in global mean sea level? *Geophys. Res. Lett.*, **39**, L18607, doi:10.1029/2012GL052885.

Chepurin, G. A., J. A. Carton, and E. Leuliette, 2014: Sea level in ocean reanalyses and tide gauges. *J. Geophys. Res. Oceans*, **119**, 147–155, doi:10.1002/2013JC009365.

Church, J. A., and N. J. White, 2011: Sea-level rise from the late 19th to the early 21st century. *Surv. Geophys.*, **32**, 585–602, doi:10.1007/s10712-011-9119-1.

Clarke, A. J., and K. H. Brink, 1985: The response of stratified, frictional flow of shelf and slope waters to fluctuating large-scale, low-frequency wind forcing. *J. Phys. Oceanogr.*, **15**, 439–453, doi:10.1175/1520-0485(1985)015<0439:TROSFF>2.0.CO;2.

Compo, G. P., and Coauthors, 2011: The Twentieth Century Reanalysis Project. *Quart. J. Roy. Meteor. Soc.*, **137**, 1–28, doi:10.1002/qj.776.

Csanady, G. T., 1982: *Circulation in the Coastal Ocean*. Springer, 279 pp.

Dangendorf, S., D. Rybski, C. Mudersbach, A. Müller, E. Kaufmann, E. Zorita, and J. Jensen, 2014: Evidence for long-term memory in sea level. *Geophys. Res. Lett.*, **41**, 5530–5537, doi:10.1002/2014GL060538.

Dee, D. P., and Coauthors, 2011: The ERA-Interim reanalysis: Configuration and performance of the data assimilation system. *Quart. J. Roy. Meteor. Soc.*, **137**, 553–597, doi:10.1002/qj.828.

Forget, G., J.-M. Campin, P. Heimbach, C. N. Hill, R. M. Ponte, and C. Wunsch, 2015: ECCO version 4: An integrated framework for non-linear inverse modeling and global ocean state estimation. *Geosci. Model Dev.*, **8**, 3071–3104, doi:10.5194/gmd-8-3071-2015.

Frankignoul, C., P. Müller, and E. Zorita, 1997: A simple model of the decadal response of the ocean to stochastic wind forcing. *J. Phys. Oceanogr.*, **27**, 1533–1546, doi:10.1175/1520-0485(1997)027<1533:ASMOTD>2.0.CO;2.

Giese, B. S., and S. Ray, 2011: El Niño variability in Simple Ocean Data Assimilation (SODA), 1871–2008. *J. Geophys. Res.*, **116**, C02024, doi:10.1029/2010JC006695.

Gill, A. E., and P. P. Niiler, 1973: The theory of the seasonal variability in the ocean. *Deep-Sea Res. Oceanogr. Abstr.*, **20**, 141–177, doi:10.1016/0011-7471(73)90049-1.

Goddard, P. B., J. Yin, S. M. Griffies, and S. Zhang, 2015: An extreme event of sea-level rise along the northeast coast of North America in 2009–2010. *Nat. Commun.*, **6**, 6346, doi:10.1038/ncomms7346.

Greatbatch, R. J., Y. Lu, and B. de Young, 1996: Application of a barotropic model to North Atlantic synoptic sea level variability. *J. Mar. Res.*, **54**, 451–469, doi:10.1357/0022240963213501.

Hannah, C. G., J. A. Shore, J. W. Loder, and C. E. Naimie, 2001: Seasonal circulation on the western and central Scotian shelf. *J. Phys. Oceanogr.*, **31**, 591–615, doi:10.1175/1520-0485(2001)031<0591:SCOTWA>2.0.CO;2.

Hernandez, F., and Coauthors, 2014: Sea level intercomparison: Initial results. *CLIVAR Exchanges*, No. 64, International CLIVAR Project Office, Southampton, United Kingdom, 18–21.

Higginson, S., K. R. Thompson, P. L. Woodworth, and C. W. Hughes, 2015: The tilt of mean sea level along the east coast of North America. *Geophys. Res. Lett.*, **42**, 1471–1479, doi:10.1002/2015GL063186.

Holgate, S. J., and Coauthors, 2013: New data systems and products at the permanent service for mean sea level. *J. Coast. Res.*, **29**, 493–504, doi:10.2112/JCOASTRES-D-12-00175.1.

Holton, J. R., 1992: *An Introduction to Dynamic Meteorology*. Academic Press, 511 pp.

Hong, B. G., W. Sturges, and A. J. Clarke, 2000: Sea level on the U.S. East Coast: Decadal variability caused by open ocean wind-curl forcing. *J. Phys. Oceanogr.*, **30**, 2088–2098, doi:10.1175/1520-0485(2000)030<2088:SLOTUS>2.0.CO;2.

Hughes, C. W., R. J. Bingham, V. Roussenov, J. Williams, and P. L. Woodworth, 2015: The effect of Mediterranean exchange flow on European time mean sea level. *Geophys. Res. Lett.*, **42**, 466–474, doi:10.1002/2014GL062654.

Ingleby, B., and M. Huddleston, 2007: Quality control of ocean temperature and salinity profiles—Historical and real-time data. *J. Mar. Syst.*, **65**, 158–175, doi:10.1016/j.jmarsys.2005.11.019.

Kalnay, E., and Coauthors, 1996: The NCEP/NCAR 40-Year Reanalysis Project. *Bull. Amer. Meteor. Soc.*, **77**, 437–471, doi:10.1175/1520-0477(1996)077<0437:TNYRP>2.0.CO;2.

Kanamitsu, M., W. Ebisuzaki, J. Woollen, S.-K. Yang, J. J. Hnilo, M. Fiorino, and G. L. Potter, 2002: NCEP–DOE AMIP-II Reanalysis (R-2). *Bull. Amer. Meteor. Soc.*, **83**, 1631–1643, doi:10.1175/BAMS-83-11-1631.

Kistler, R., and Coauthors, 2001: The NCEP–NCAR 50-Year Reanalysis: Monthly means CD-ROM and documentation. *Bull. Amer. Meteor. Soc.*, **82**, 247–267, doi:10.1175/1520-0477(2001)082<0247:TNNYRM>2.3.CO;2.

Köhl, A., 2015: Evaluation of the GECCO2 ocean synthesis: Transports of volume, heat and freshwater in the Atlantic. *Quart. J. Roy. Meteor. Soc.*, **141**, 166–181, doi:10.1002/qj.2347.

Kopp, R. E., 2013: Does the mid-Atlantic United States sea level acceleration hot spot reflect ocean dynamic variability? *Geophys. Res. Lett.*, **40**, 3981–3985, doi:10.1002/grl.50781.

——, and Coauthors, 2014: Probabilistic 21st and 22nd century sea-level projections at a global network of tide-gauge sites. *Earth's Future*, **2**, 383–406, doi:10.1002/2014EF000239.

Landerer, F. W., J. H. Jungclaus, and J. Marotzke, 2007: Regional dynamic and steric sea level change in response to the IPCC-A1B scenario. *J. Phys. Oceanogr.*, **37**, 296–312, doi:10.1175/JPO3013.1.

Levermann, A., A. Griesel, M. Hofmann, M. Montoya, and S. Rahmstorf, 2005: Dynamic sea level changes following changes in the thermohaline circulation. *Climate Dyn.*, **24**, 347–354, doi:10.1007/s00382-004-0505-y.

Li, Y., R. Ji, P. S. Fratantoni, C. Chen, J. A. Hare, C. S. Davis, and R. C. Beardsley, 2014: Wind-induced interannual variability of sea level slope, along-shelf flow, and surface salinity on the northwest Atlantic shelf. *J. Geophys. Res. Oceans*, **119**, 2462–2479, doi:10.1002/2013JC009385.

Little, C. M., R. M. Horton, R. E. Kopp, M. Oppenheimer, and S. Yip, 2015: Uncertainty in twenty-first-century CMIP5 sea level projections. *J. Climate*, **28**, 838–852, doi:10.1175/JCLI-D-14-00453.1.

Madec, G., 2008: NEMO reference manual, ocean dynamics component: NEMO-OPA, preliminary version. Note du Pôle de modélisation Rep. 27.

Marshall, J., A. Adcroft, C. Hill, L. Perelman, and C. Heisey, 1997: A finite-volume, incompressible Navier Stokes model for studies of the ocean on parallel computers. *J. Geophys. Res.*, **102**, 5753–5766, doi:10.1029/96JC02775.

McCarthy, G. D., I. D. Haigh, J. J.-M. Hirschi, J. P. Grist, and D. A. Smeed, 2015: Ocean impact on decadal Atlantic climate variability revealed by sea-level observations. *Nature*, **521**, 508–510, doi:10.1038/nature14491.

Miller, L., and B. C. Douglas, 2007: Gyre-scale atmospheric pressure variations and their relation to 19th and 20th century sea level rise. *Geophys. Res. Lett.*, **34**, L16602, doi:10.1029/2007GL030862.

Mogensen, K., M. A. Balmaseda, and A. T. Weaver, 2012: The NEMOVAR ocean data assimilation system as implemented in the ECMWF ocean analysis for system 4. ECMWF Tech. Memo. 668, 59 pp.

Passaro, M., P. Cipollini, and J. Benveniste, 2015: Annual sea level variability of the coastal ocean: The Baltic Sea–North Sea transition zone. *J. Geophys. Res. Oceans*, **120**, 3061–3078, doi:10.1002/2014JC010510.

Pedlosky, J., 1992: *Geophysical Fluid Dynamics*. Springer, 710 pp.

Permanent Service for Mean Sea Level, 2015: Tide gauge data. Permanent Service for Mean Sea Level, accessed 16 February 2015. [Available online at http://www.psmsl.org/data/obtaining/.]

Piecuch, C. G., and R. M. Ponte, 2015: Inverted barometer contributions to recent sea level changes along the northeast coast of North America. *Geophys. Res. Lett.*, **42**, 5918–5925, doi:10.1002/2015GL064580.

Poli, P., and Coauthors, 2013: The data assimilation system and initial performance evaluation of the ECMWF pilot reanalysis of the 20th-century assimilating surface observations only (ERA-20C). ERA Rep. Series 14, 62 pp.

Ponte, R. M., 1993: Variability in a homogeneous global ocean forced by barometric pressure. *Dyn. Atmos. Oceans*, **18**, 209–234, doi:10.1016/0377-0265(93)90010-5.

——, 2006: Low-frequency sea level variability and the inverted barometer effect. *J. Atmos. Oceanic Technol.*, **23**, 619–629, doi:10.1175/JTECH1864.1.

Rayner, N. A., D. E. Parker, E. B. Horton, C. K. Folland, L. V. Alexander, D. P. Rowell, E. C. Kent, and A. Kaplan, 2003: Global analyses of sea surface temperature, sea ice, and night marine air temperature since the late nineteenth century. *J. Geophys. Res.*, **108**, 4407, doi:10.1029/2002JD002670.

Saba, V. S., and Coauthors, 2016: Enhanced warming of the northwest Atlantic Ocean under climate change. *J. Geophys. Res. Oceans*, **121**, 118–132, doi:10.1002/2015JC011346.

Sallenger, A. H., K. S. Doran, and P. A. Howd, 2012: Hotspot of accelerated sea-level rise on the Atlantic coast of North America. *Nat. Climate Change*, **2**, 884–888, doi:10.1038/nclimate1597.

Sandstrom, H., 1980: On the wind-induced sea level changes on the Scotian shelf. *J. Geophys. Res.*, **85**, 461–468, doi:10.1029/JC085iC01p00461.

Slangen, A. B. A., and Coauthors, 2014: Projecting twenty-first century regional sea-level changes. *Climatic Change*, **124**, 317–332, doi:10.1007/s10584-014-1080-9.

Smith, R. D., J. K. Dukowicz, and R. C. Malone, 1992: Parallel ocean general circulation modeling. *Physica D*, **60**, 38–61, doi:10.1016/0167-2789(92)90225-C.

Taylor, K. E., 2001: Summarizing multiple aspects of model performance in a single diagram. *J. Geophys. Res.*, **106**, 7183–7192, doi:10.1029/2000JD900719.

——, R. J. Stouffer, and G. A. Meehl, 2012: An overview of CMIP5 and the experimental design. *Bull. Amer. Meteor. Soc.*, **93**, 485–498, doi:10.1175/BAMS-D-11-00094.1.

Thompson, K. R., 1986: North Atlantic sea-level and circulation. *Geophys. J. Int.*, **87**, 15–32, doi:10.1111/j.1365-246X.1986.tb04543.x.

Thompson, P. R., and G. T. Mitchum, 2014: Coherent sea level variability on the North Atlantic western boundary. *J. Geophys. Res. Oceans*, **119**, 5676–5689, doi:10.1002/2014JC009999.

Uppala, S. M., and Coauthors, 2005: The ERA-40 Re-Analysis. *Quart. J. Roy. Meteor. Soc.*, **131**, 2961–3012, doi:10.1256/qj.04.176.

Vellinga, M., and R. A. Wood, 2008: Impacts of thermohaline circulation shutdown in the twenty-first century. *Climatic Change*, **91**, 43–63, doi:10.1007/s10584-006-9146-y.

Vinogradov, S. V., and R. M. Ponte, 2011: Low-frequency variability in coastal sea level from tide gauges and altimetry. *J. Geophys. Res.*, **116**, C07006, doi:10.1029/2011JC007034.

Vinogradova, N. T., R. M. Ponte, and D. Stammer, 2007: Relation between sea level and bottom pressure and the vertical dependence of oceanic variability. *Geophys. Res. Lett.*, **34**, L03608, doi:10.1029/2006GL028588.

von Storch, H., and F. W. Zwiers, 1999: *Statistical Analysis in Climate Research*. Cambridge University Press, 496 pp.

Woodruff, S. D., and Coauthors, 2011: ICOADS release 2.5: Extensions and enhancements to the surface marine meteorological archive. *Int. J. Climatol.*, **31**, 951–967, doi:10.1002/joc.2103.

Woodworth, P. L., M. Á. M. Maqueda, V. M. Roussenov, R. G. Williams, and C. W. Hughes, 2014: Mean sea-level variability along the northeast American Atlantic coast and the roles of the wind and the overturning circulation. *J. Geophys. Res. Oceans*, **119**, 8916–8935, doi:10.1002/2014JC010520.

Wunsch, C., 2002: What is the thermohaline circulation? *Science*, **298**, 1179–1181, doi:10.1126/science.1079329.

Xue, Y., B. Huang, Z.-Z. Hu, A. Kumar, C. Wen, D. Behringer, and S. Nadiga, 2011: An assessment of oceanic variability in the NCEP Climate Forecast System Reanalysis. *Climate Dyn.*, **37**, 2511–2539, doi:10.1007/s00382-010-0954-4.

Yin, J., and P. B. Goddard, 2013: Oceanic control of sea level rise patterns along the East Coast of the United States. *Geophys. Res. Lett.*, **40**, 5514–5520, doi:10.1002/2013GL057992.

——, M. E. Schlesinger, and R. J. Stouffer, 2009: Model projections of rapid sea-level rise on the northeast coast of the United States. *Nat. Geosci.*, **2**, 262–266, doi:10.1038/ngeo462.